Design and evalution of frequency-warped sigma delta modulators[1]

Ludovico Ausiello[2], Toon van Waterschoot[3], and Marc Moonen[4]

April 2008.
Submitted for publication in *IEEE Trans. Signal Process.*

[1]This report is available by anonymous ftp from *ftp.esat.kuleuven.be* in the directory *pub/sista/vanwaterschoot/reports/07-190.pdf*

[2]ARCES, University of Bologna, Via Toffano 2, 40125 Bologna, Italy, Tel. +39 051 2095400, Fax +39 051 2095410, E-mail: *lausiello@arces.unibo.it*. This research work was carried out at the ESAT laboratory of the Katholieke Universiteit Leuven, in the frame of the Edith Program, the K.U.Leuven Research Council: CoE EF/05/006 Optimization in Engineering (OPTEC), and the Belgian Programme on Interuniversity Attraction Poles, initiated by the Belgian Federal Science Policy Office IUAP P6/04 (DYSCO, "Dynamical systems, control and optimization", 2007-2011) and was supported by the Marie Curie Early Stage Training No. 504125 and the Institute for the Promotion of Innovation through Science and Technology in Flanders (IWT-Vlaanderen). The scientific responsibility is assumed by its authors.

[3]K.U.Leuven, Dept. of Electrical Engineering (ESAT), Research group SCD(SISTA), Kasteelpark Arenberg 10, B-3001 Leuven, Belgium, Tel. +32 16 321927, Fax +32 16 321970, WWW: *http://homes.esat.kuleuven.be/∼tvanwate*. E-mail: *toon.vanwaterschoot@esat.kuleuven.be*. Toon van Waterschoot is a Research Assistant with the Institute for the Promotion of Innovation through Science and Technology in Flanders (IWT-Vlaanderen).

[4]K.U.Leuven, Dept. of Electrical Engineering (ESAT), Research group SCD(SISTA), Kasteelpark Arenberg 10, B-3001 Leuven, Belgium, Tel. +32 16 321060, Fax +32 16 321970, WWW: *http://www.esat.kuleuven.be/sista-cosic-docarch*. E-mail: *marc.moonen@esat.kuleuven.be*.

Design and Evaluation of Frequency-Warped Sigma Delta Modulators†

Ludovico Ausiello*[1], Toon van Waterschoot[2], and Marc Moonen[3]

Abstract

In this paper, a novel Sigma Delta Modulator (SDM) design procedure is presented, with specific interest in developing a general model using a frequency-warped modulator filter structure. The proposed design procedure is based on warping the SDM noise transfer function (NTF) using the bilinear all-pass transformation, and allows for some flexibility in the way the signal transfer function (STF) is affected by the warping. Both the analytical representation and a practical architecture implementation are described for first-order and high-order frequency-warped modulator filters. Topology examples are included to illustrate the effect of frequency warping on the STF and NTF frequency responses. For the high-order case, a realizable warped filter structure without algebraic signal loops is derived. Simulation results using sinusoidal test signals indicate a superior performance of the frequency-warped SDMs as compared to the traditional topologies.

I. Introduction

A Sigma Delta Modulator (SDM) is a non-linear device widely used in analog-to-digital conversion (ADC) to achieve a high resolution without requiring high-precision analog components. Its typical output stream has two fundamental characteristics, namely a few-bit wordlength for the samples representing the amplitude of the incoming signal and a very high sampling rate. A high signal-to-noise ratio (SNR) can

†EDICS: DSP-FILT (Filter design and structures), NSP-NLIN (Nonlinear signals and systems)

*Corresponding author

[1]ARCES, University of Bologna, Via Toffano 2, 40125 Bologna, Italy, Tel. +39 051 2095400, Fax +39 051 2095410, E-mail lausiello@arces.unibo.it

[2]Katholieke Universiteit Leuven, ESAT-SCD, Kasteelpark Arenberg 10, B-3001 Leuven, Tel. +32 16 321927, Fax +32 16 321970, E-mail toon.vanwaterschoot@esat.kuleuven.be

[3]Katholieke Universiteit Leuven, ESAT-SCD, Kasteelpark Arenberg 10, B-3001 Leuven, Tel. +32 16 321060, Fax +32 16 321970, E-mail marc.moonen@esat.kuleuven.be

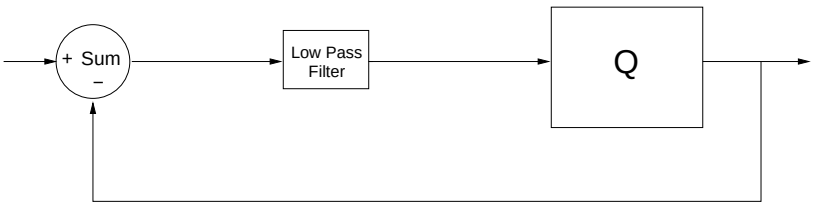

Figure 1. Block diagram for a Sigma Delta Modulator.

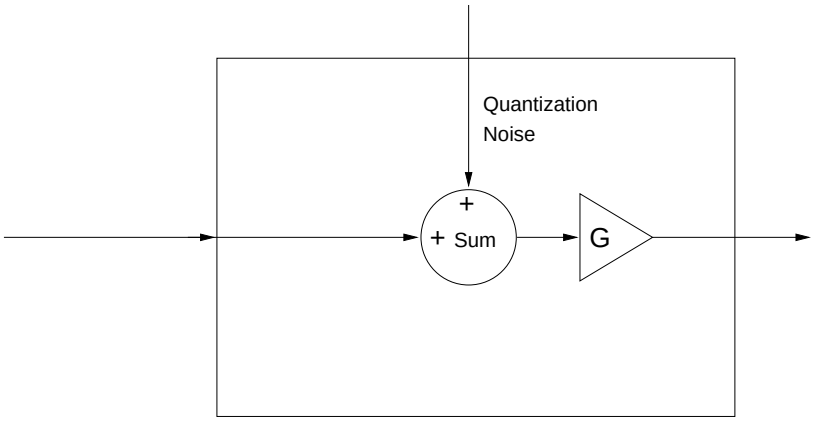

Figure 2. Noise model for the quantizer Q.

be obtained by increasing the oversampling ratio (OSR) and by decreasing the noise power in the band of interest using specific filter topologies [1]-[5]. As seen in Fig. 1, the building blocks of the system are a low-pass filter, a quantizer (denoted by Q), and a negative feedback loop. The usual linear model for the quantizer (which actually makes the system non-linear) consists of an additive noise source and a gain (see Fig. 2). The noise source represents the quantization noise, introduced by the quantizer.

We can think of the whole SDM as a device in which the feedback signal represents the quantization noise, while the low-pass filter in the feedforward path is designed to cancel it, more specifically to process its frequency content, moving it to a part of the spectrum that is not important for the specific application. For example, in audio ADC, the quantization noise is shifted to a frequency interval that is higher than the audio band. The role of the low-pass modulator filter is, consequently, of fundamental importance to achieve the desired performance in terms of SNR and signal-to-noise-and-distortion ratio (SINAD). With the intent of increasing the performance of a SDM without affecting the complexity of the low-pass modulator filter, a new design procedure for the modulator filter is proposed in this paper, which is based on the theory of frequency warping [6]. The resulting SDM is expected to achieve a better

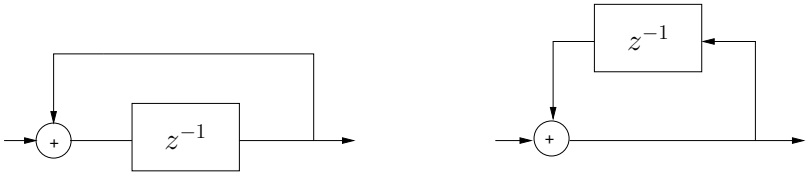

Figure 3. SDM low-pass filter building blocks: first-order integrator (left) and resonator (right).

SNR and SINAD compared to a traditional topology of the same order, due to an increased frequency selectivity of the warped modulator filter.

The two traditional building blocks for a SDM low-pass filter are a delay block surrounded by a local feedback loop (i.e., a first-order integrator) and a direct path with a delay in the local feedback loop (i.e., a first-order resonator), see Fig. 3. As stated in [7] we can immediately embed a frequency warping effect into a normal FIR or IIR filter by replacing every delay block with a bilinear all-pass block, with warping parameter $\lambda \in (-1, 1)$:

$$z^{-1} \rightarrow \frac{z^{-1} - \lambda}{1 - \lambda z^{-1}}. \tag{1}$$

This procedure is often used in audio filter design and leads to a peculiar effect: it maps the frequency axis onto itself, with

$$z^{-1} = e^{j2\pi k} \rightarrow \frac{z^{-1} - \lambda}{1 - \lambda z^{-1}} = e^{j2\pi k}, \quad k = 0, 1, \ldots \tag{2}$$

For $\lambda > 0$, the part of the spectrum lower than the so-called turning point frequency f_{TP} is expanded and the higher part is compressed (and vice versa, for $\lambda < 0$), with f_{TP} defined as [7]

$$f_{\text{TP}} = \frac{f_S}{2\pi} \arccos(\lambda) \tag{3}$$

and f_S the sampling frequency.

As already proposed in lossy audio coding techniques [8], a non-uniform representation of the frequency axis can be a powerful tool for increasing the frequency resolution in the low part of the spectrum, to emulate human hearing, which indeed approximately has a constant-Q analysis capability [9]. By embedding this feature directly into the SDM, we can expect a better performance because of the more selective noise shaping. In audio applications, it is usually preferred to use a high symbol rate (i.e., a high oversampling ratio (OSR)) and relatively simple low-pass filters, made up of only one or two integrator stages. The usage of frequency warping in a first-order SDM architecture was described in [10] and yields an SDM design with a lower noise transfer function (NTF) Nyquist gain (also called “out-of-band gain”), which is important for stability reasons [11]. Moreover, the signal transfer function (STF) is shaped to be

more frequency selective. These advantages can be achieved without significantly changing the complexity of the filter. On the other hand, there are other applications, such as telecommunication applications, in which the applicable OSR is limited due to the large signal bandwidth, hence the use of higher-order modulator topologies is required [12]. In this paper, we extend the first-order frequency-warped SDM design proposed in [10] to the high-order case with the aim of improving the SNR performance without increasing the SDM order.

The paper is organized as follows. In Section II, we briefly introduce the notation used in the rest of the paper. Section III provides a brief review of the design of first-order frequency-warped SDMs as proposed in [10]. Replacing directly the integrator in the traditional first-order SDM filter offers some cues to reflect on. First of all, we are warping the NTF and STF simultaneously and, more subtle, we are now introducing a direct path from the input to the quantizer and consequently to the output. This direct path is not present in the original implementation and may introduce a realizability problem if there is no delay block in the feedback path such that an algebraic loop is constructed. We will therefore propose a design procedure in which first the NTF is warped and subsequently scaled to avoid a direct path from the input to the quantizer. In a second step, a decision has to be made on how the STF will be affected by the frequency warping. In particular, we will propose two first-order warped SDM topologies sharing the same NTF, but having a different STF. We will also mention the predicted SNR results obtained in [10], for both white noise and sinusoidal input signals. In Section IV, the design procedure proposed in Section III is generalized to high-order SDM filters. This is illustrated for the cascade-of-integrators feedforward (CIFF) SDM topology [5, Ch. 4]. Again, we start by warping and scaling the NTF, and then propose two different ways in which the warping may alter the STF, leading to two high-order frequency-warped SDM topologies. Since the local resonator feedback loops, which may be present in the traditional CIFF topology, produce algebraic loops after frequency warping, we also describe a method, inspired by [13], for transforming an unrealizable delay-free local resonator feedback loop into a realizable structure. Finally, in Section V, we present some simulation results of first-order and fifth-order frequency-warped SDMs and compare them to traditional SDMs in terms of SNR. Section VI concludes the paper.

II. NOTATION

In this Section, an analytical model is presented which can be used for both first-order and high-order SDMs. The notation used is adopted from [11]. We can represent a SDM as a two-input, single-output device as depicted in Fig. 4.

Here, $G(z)$ denotes the STF and $H(z)$ the NTF. $U(z)$ is the input signal and $V(z)$ is the encoded

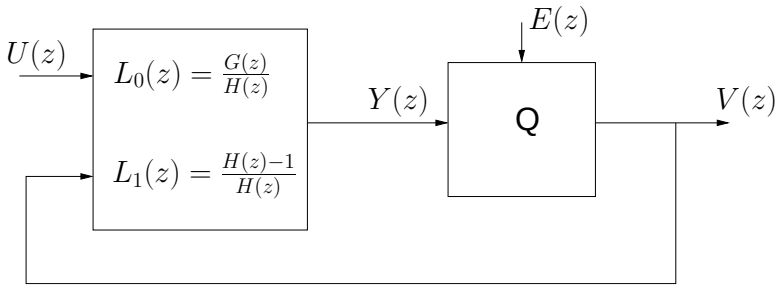

Figure 4. General block diagram of a single-quantizer SDM.

output. If we define the quantization error signal as $E(z) = V(z) - Y(z)$, we can present the classical input-output relation for the modulator, that is

$$V(z) = G(z)U(z) + H(z)E(z) \tag{4}$$

and the so-called loop filters are defined as

$$L_0(z) = \frac{G(z)}{H(z)} \tag{5}$$

and

$$L_1 = \frac{H(z) - 1}{H(z)}. \tag{6}$$

It is important to remember that in this simplified linear model the noise $E(z)$ is actually signal-dependent.

III. First-Order Frequency-Warped SDM Design

A. Design Procedure

To illustrate the concept of designing a frequency-warped SDM, we start by considering the first-order case [10]. The noise shaping function is then a first-order pure differentiator, with a transfer function

$$H^{(1)}(z) = 1 - z^{-1} \tag{7}$$

in which the superscript is included to distinguish between the first-order and high-order case (see Section IV). The NTF can be warped by replacing the complex variable z with the bilinear all-pass function $\frac{z-\lambda}{1-\lambda z}$ (or, equivalently, by replacing z^{-1} with $\frac{z^{-1}-\lambda}{1-\lambda z^{-1}}$), i.e.,

$$H^{(1)}(z, \lambda) = 1 - \frac{z^{-1} - \lambda}{1 - \lambda z^{-1}} = \frac{(1+\lambda)(1 - z^{-1})}{1 - \lambda z^{-1}}. \tag{8}$$

As pointed out in [11], the NTF should always be scaled such that the first tap of its impulse response is 1. This is necessary to assure that the L_1 loop filter contains at least one pure time delay, hence avoiding

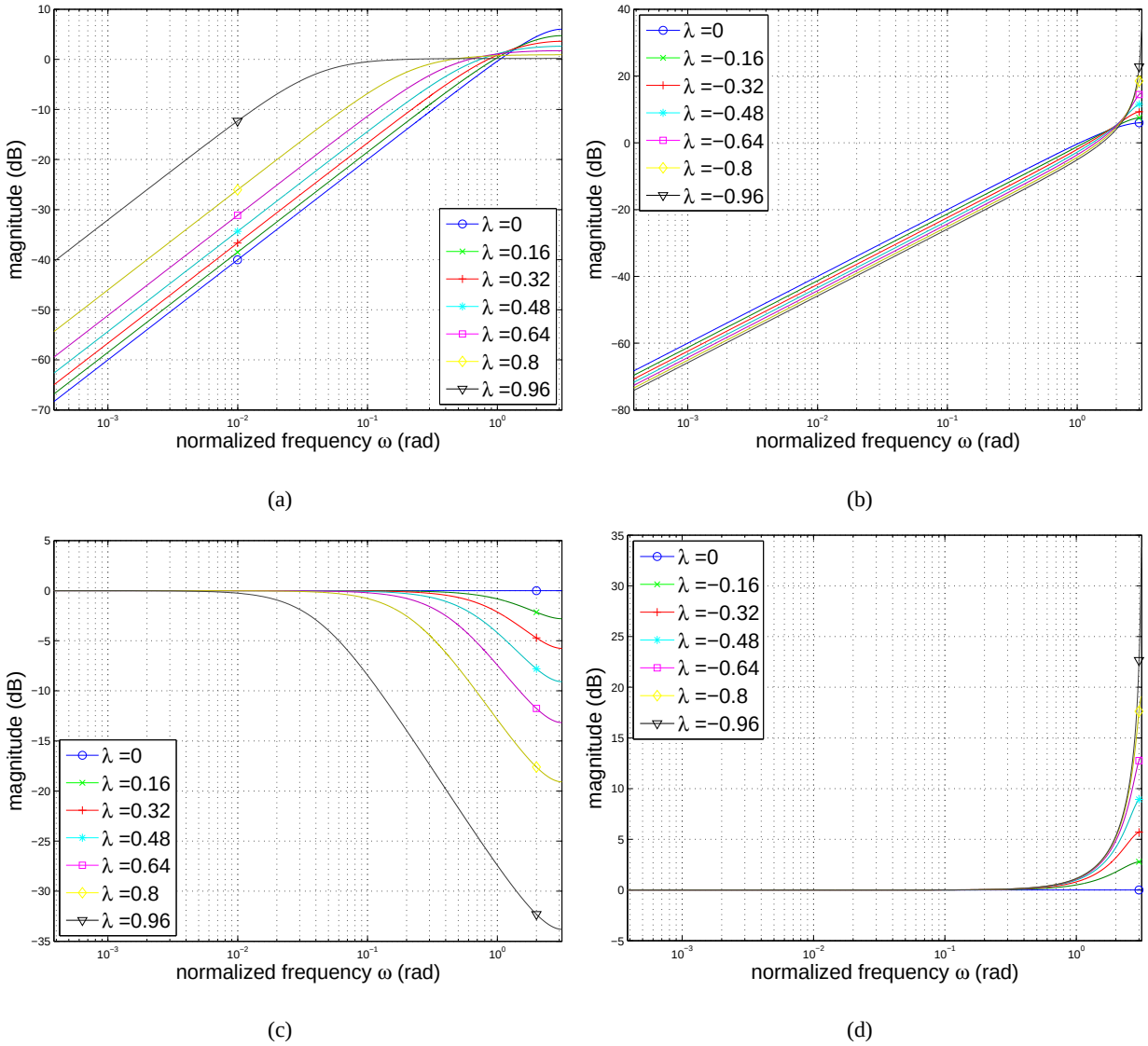

Figure 5. First-order frequency-warped SDM: (a) NTF magnitude response ($\lambda \geq 0$), (b) NTF magnitude response ($\lambda \leq 0$), (c) STF magnitude response, (topology I, $\lambda \geq 0$), (d) STF magnitude response (topology I, $\lambda \leq 0$).

an algebraic loop in the closed-loop SDM scheme. The first tap of the impulse response of $H^{(1)}(z,\lambda)$ equals $(1+\lambda)$, hence the desired warped and scaled NTF is obtained by dividing the transfer function in (8) by $(1+\lambda)$, i.e.,

$$\tilde{H}^{(1)}(z,\lambda) = \frac{1-z^{-1}}{1-\lambda z^{-1}}. \tag{9}$$

The magnitude response of $\tilde{H}^{(1)}(z,\lambda)$ is shown in Figs. 5(a) and 5(b) for positive and negative warping parameters, respectively.

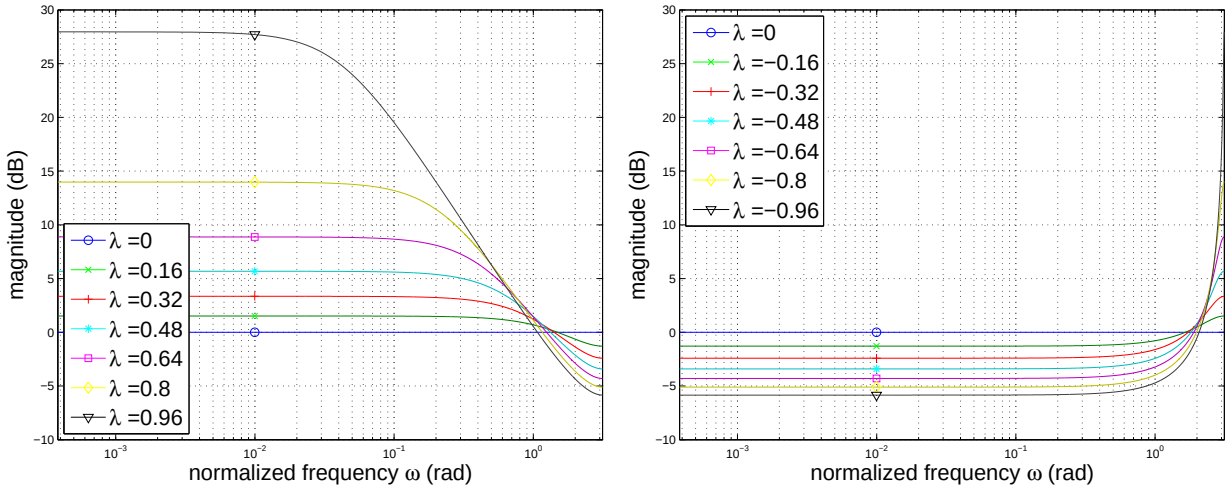

(a) (b)

Figure 6. First-order frequency-warped SDM: (a) STF magnitude response (topology II, $\lambda \geq 0$), (b) STF magnitude response (topology II, $\lambda \leq 0$).

The corresponding warped loop filter $\tilde{L}_1^{(1)}(z,\lambda)$ can now be calculated as follows:

$$\tilde{L}_1^{(1)}(z,\lambda) = \frac{\tilde{H}^{(1)}(z,\lambda) - 1}{\tilde{H}^{(1)}(z,\lambda)} = -(1-\lambda)\frac{z^{-1}}{1-z^{-1}}. \tag{10}$$

At this point the warped SDM design allows for some freedom in deciding how the frequency warping will affect the STF $G^{(1)}(z)$. The effect on $G^{(1)}(z)$ follows directly from the choice of the loop filter $\tilde{L}_0^{(1)}(z,\lambda)$.

A *first possibility* is to constrain the warped loop filters $\tilde{L}_0^{(1)}(z,\lambda)$ and $\tilde{L}_1^{(1)}(z,\lambda)$ to obey the same relationship as they do in the non-warped case, i.e.,

$$L_0^{(1)}(z) = -L_1^{(1)}(z) \Rightarrow \tilde{L}_0^{(1)}(z,\lambda) = -\tilde{L}_1^{(1)}(z,\lambda). \tag{11}$$

This choice leads to

$$\tilde{L}_{0,\mathrm{I}}^{(1)}(z,\lambda) = (1-\lambda)\frac{z^{-1}}{1-z^{-1}} \tag{12}$$

which corresponds to the first-order SDM topology shown in Fig. 7, denoted as topology I. It can be seen that the warping merely comes down to adding a gain factor $(1-\lambda)$ in the SDM forward path. The warped STF $\tilde{G}_{\mathrm{I}}^{(1)}(z,\lambda)$ is in this case given by

$$\tilde{G}_{\mathrm{I}}^{(1)}(z,\lambda) = \tilde{L}_{0,\mathrm{I}}^{(1)}(z,\lambda)\tilde{H}^{(1)}(z,\lambda) = (1-\lambda)\frac{z^{-1}}{1-\lambda z^{-1}} \tag{13}$$

which is a high-pass filter if $\lambda < 0$, a low-pass filter if $\lambda > 0$, and a pure time delay if $\lambda = 0$. The STF magnitude response is plotted in Figs. 5(c) and 5(d) for positive and negative warping parameters,

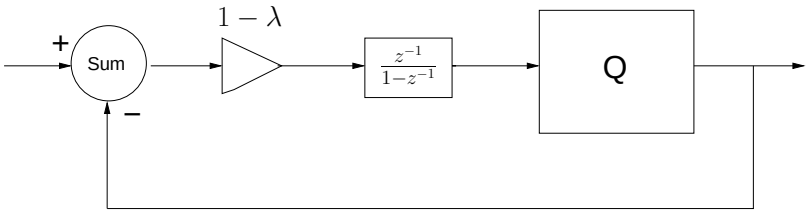

Figure 7. First-order frequency-warped SDM topology I ($\tilde{L}_0^{(1)}(z,\lambda) = -\tilde{L}_1^{(1)}(z,\lambda)$).

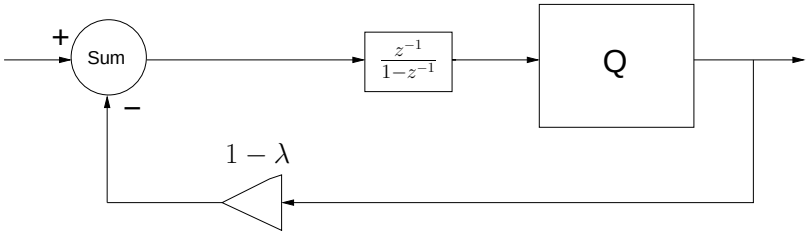

Figure 8. First-order frequency-warped SDM topology II ($\tilde{L}_0^{(1)}(z,\lambda) = L_0^{(1)}(z)$).

respectively. In our application, the positive range of the warping parameter is more interesting, because of the similarity to human hearing. Furthermore, a positive value of λ yields a low-pass STF, even in the first-order case (where the STF usually has a flat magnitude response).

A *second possibility* for completing the design of a first-order warped SDM is to constrain $\tilde{L}_0^{(1)}(z,\lambda)$ to be equal to the loop filter $L_0^{(1)}(z)$ in the non-warped first-order SDM, i.e.,

$$\tilde{L}_{0,\mathrm{II}}^{(1)}(z,\lambda) = \frac{z^{-1}}{1-z^{-1}}. \tag{14}$$

which leads to

$$\tilde{G}_{\mathrm{II}}^{(1)}(z,\lambda) = \frac{z^{-1}}{1-\lambda z^{-1}}. \tag{15}$$

The resulting topology, denoted as topology II, is shown in Fig. 8. It only differs from topology I in the position of the gain factor $(1-\lambda)$, which is now in the feedback path. Obviously, the NTF $\tilde{H}^{(1)}(z,\lambda)$ is the same for both topologies, whereas the STF $\tilde{G}_{\mathrm{II}}^{(1)}(z,\lambda)$ is a scaled version of the STF $\tilde{G}_{\mathrm{I}}^{(1)}(z,\lambda)$ in (13). The scaling is such that the gain at dc increases for increasing λ, whereas for topology I it is equal to 0 dB for all values of λ. This can be seen from the topology II STF magnitude response, plotted in Figs. 6(a) and 6(b) for positive and negative values of λ, respectively.

We should mention that, while the warped and scaled first-order NTF in (9) can be considered as a special case of the NTF of the so-called enhanced first-order SDM [12], the STFs proposed in (13) and (15) are not special cases of the STF in [12], due to the absence of a delay in the SDM feedback path.

As a consequence, the results on SNR and the stability analysis presented in [12], cannot be applied to the first-order frequency-warped SDM topologies considered here.

The implementation of the first-order frequency-warped SDM topologies only requires one additional multiplier, compared to the traditional implementation, either in the forward path or in the feedback path, hence the increase in computational complexity or hardware cost is marginal.

B. SNR Prediction

In [10], the SNR was predicted using the analytical model for the first-order frequency-warped SDM, and given by (for $\lambda \neq 0$)):

$$\text{SNR}_{\text{I}}(\text{WN}) = 10\log_{10}\frac{\sigma_x^2}{\sigma_e^2}\lambda\frac{1-\lambda}{1+\lambda}\frac{\arctan\left(\frac{1+\lambda}{1-\lambda}\tan\frac{\pi}{2\text{OSR}}\right)}{\frac{\pi}{2\text{OSR}}-\frac{1-\lambda}{1+\lambda}\arctan\left(\frac{1+\lambda}{1-\lambda}\tan\frac{\pi}{2\text{OSR}}\right)} \tag{16}$$

$$\text{SNR}_{\text{II}}(\text{WN}) = 10\log_{10}\frac{\sigma_x^2}{\sigma_e^2}\frac{\lambda}{1-\lambda^2}\frac{\arctan\left(\frac{1+\lambda}{1-\lambda}\tan\frac{\pi}{2\text{OSR}}\right)}{\frac{\pi}{2\text{OSR}}-\frac{1-\lambda}{1+\lambda}\arctan\left(\frac{1+\lambda}{1-\lambda}\tan\frac{\pi}{2\text{OSR}}\right)} \tag{17}$$

$$\text{SNR}_{\text{I}}(\text{SIN}) = 10\log_{10}\frac{\sigma_x^2}{\sigma_e^2}\lambda\frac{(1-\lambda)^2}{1-2\lambda\cos\omega_0+\lambda^2}\frac{1}{1-\frac{2\text{OSR}}{\pi}\frac{1-\lambda}{1+\lambda}\arctan\left(\frac{1+\lambda}{1-\lambda}\tan\frac{\pi}{2\text{OSR}}\right)} \tag{18}$$

$$\text{SNR}_{\text{II}}(\text{SIN}) = 10\log_{10}\frac{\sigma_x^2}{\sigma_e^2}\frac{\lambda}{1-2\lambda\cos\omega_0+\lambda^2}\frac{1}{1-\frac{2\text{OSR}}{\pi}\frac{1-\lambda}{1+\lambda}\arctan\left(\frac{1+\lambda}{1-\lambda}\tan\frac{\pi}{2\text{OSR}}\right)} \tag{19}$$

for topologies I and II, and in case of white noise (WN) and sinusoidal (SIN) input signals (with radial frequency $\omega_0 \in [0, \pi/\text{OSR}]$), respectively.

The predicted SNR is plotted versus the warping parameter $\lambda \in (-1, 1)$ in Fig. 9 for $\sigma_x^2/\sigma_e^2 = 1$, OSR $= 64$, $f_B = 24$ kHz, and $f_0 = 1$ kHz (such that $\omega_0 = (f_0/f_B)(\pi/\text{OSR}) = 2.0453e-3$ rad). For both signal types, we observe that the SNR of topology I decreases dramatically as $\lambda \to 1$, while it increases somewhat as $\lambda \to -1$. On the other hand, the SNR of topology II is predicted to increase strongly for $\lambda \to 1$, while it remains more or less constant for other values of λ. This behavior could be expected by examining the NTF and STF magnitude responses in Figs. 5 and 6. The warped NTF magnitude response rises significantly in the signal band at high OSRs when $\lambda \to 1$ (e.g., for $\lambda = 0.8$, the NTF magnitude response is 10 dB larger than the non-warped NTF response if $\omega < 3 \cdot 10^{-1}$ rad, corresponding to the entire signal band for OSRs larger than 10, see Fig. 5(a)). On the other hand, the STF magnitude response remains constant or even decreases (for positive λ) within the signal band for the warped SDM topology I, see Fig. 5(c), which obviously leads to a loss of SNR. In contrast, the STF magnitude response of topology II shows a boost in the signal band, which increases as $\lambda \to 1$, and which (over)compensates for the increase in the NTF response, see Fig. 6(a). From this analysis,

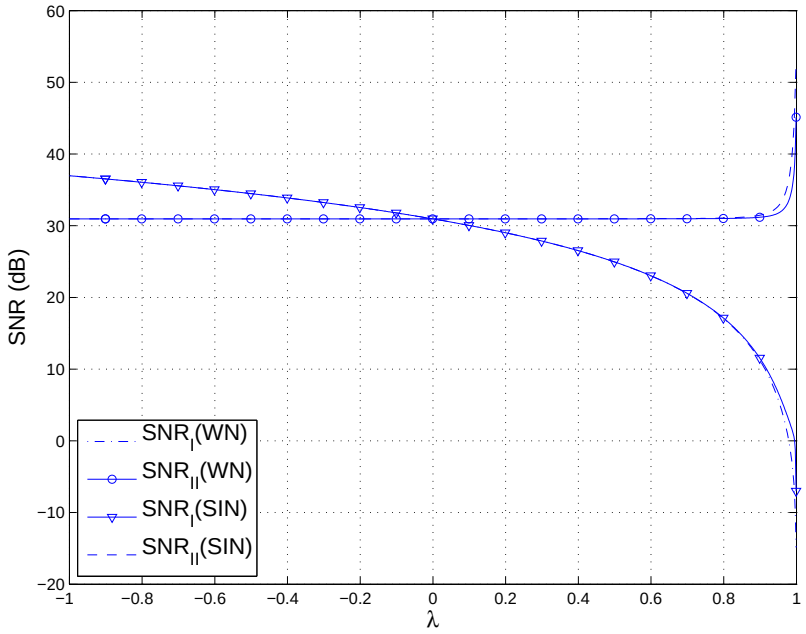

Figure 9. Predicted SNR vs. warping parameter for first-order frequency-warped SDM topologies I and II (WN = white noise input, SIN = sinusoidal input).

topology II with the positive range of the warping parameter is expected to be most promising in terms of SNR improvement. This observation will be confirmed by simulation results in Section V-A.

IV. High-Order Frequency-Warped SDM Design

A. Design Procedure

The design procedure outlined in Section III is now generalized to the case of high-order SDMs. The high-order frequency-warped SDM design is illustrated for a commonly used SDM topology, namely the cascade-of-integrators feedforward (CIFF) form [5, Ch. 4]. It should however be stressed that the design procedure is also applicable to other topologies.

High-order SDM filters generally consist of two types of building blocks: first-order integrators and first-order resonators [5, Ch. 4]. Warping the NTF of a high-order SDM can be achieved by replacing these building blocks by their warped counterparts, i.e., the first-order warped integrator

$$\frac{z^{-1}}{1-z^{-1}} \rightarrow \frac{z^{-1}-\lambda}{(1+\lambda)(1-z^{-1})} = \frac{1}{1+\lambda}\Big(\underbrace{\frac{z^{-1}}{1-z^{-1}}}_{\text{integrator}} - \lambda \underbrace{\frac{1}{1-z^{-1}}}_{\text{resonator}}\Big) \tag{20}$$

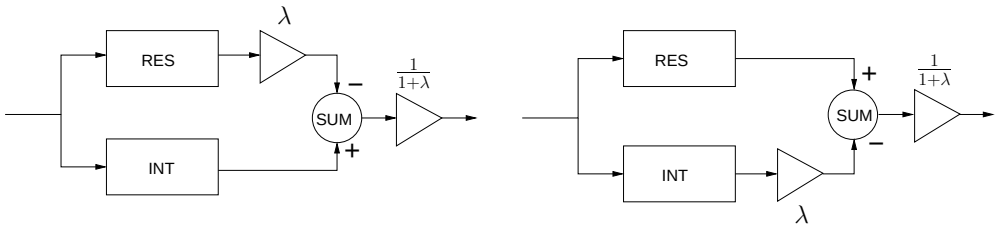

Figure 10. Parallel connections of a resonator and an integrator with appropriate scaling constitute the building blocks of the frequency-warped SDM filter.

and the first-order warped resonator

$$\frac{1}{1-z^{-1}} \rightarrow \frac{1-\lambda z^{-1}}{(1+\lambda)(1-z^{-1})} = \frac{1}{1+\lambda}\Big(\underbrace{\frac{1}{1-z^{-1}}}_{\text{resonator}} - \lambda \underbrace{\frac{z^{-1}}{1-z^{-1}}}_{\text{integrator}}\Big). \tag{21}$$

It is observed that the frequency warping of the first-order integrator and resonator functions comes down to replacing these functions by a parallel connection of a first-order integrator-resonator pair, scaled with $(1+\lambda)^{-1}$, and in which the contribution of either the resonator or the integrator is weighted with the negative warping parameter $-\lambda$ (see Fig. 10).

Consider the N-th order CIFF topology, illustrated for $N=5$ in Fig. 11. We will only deal with odd SDM orders, yet the design can easily be extended to the even order case. The NTF for this topology can be written as follows,

$$H^{(N)}(z) = \frac{1}{1+\sum_{k=1}^{N} a_k \Big(\frac{z^{-1}}{1-z^{-1}}\Big)^{p(k)} \prod_{j=1}^{\frac{k-p(k)}{2}} \frac{z^{-2}}{(1-z^{-1})^2 - g_j z^{-2}}} \tag{22}$$

where a_k are the feedforward coefficients, g_j are the coefficients of the local resonator feedback loops, and the parity function $p(k)$ is defined as

$$p(k) = \begin{cases} 0 & \text{if } k \text{ is even} \\ 1 & \text{if } k \text{ is odd} \end{cases} \tag{23}$$

Substituting (20) in the NTF transfer function (22) yields the following expression for the warped NTF:

$$H^{(N)}(z,\lambda) = \frac{1}{1+\sum_{k=1}^{N} a_k \Big(\frac{z^{-1}-\lambda}{(1+\lambda)(1-z^{-1})}\Big)^{p(k)} \prod_{j=1}^{\frac{k-p(k)}{2}} \frac{(z^{-1}-\lambda)^2}{(1+\lambda)^2(1-z^{-1})^2 - g_j(z^{-1}-\lambda)^2}}. \tag{24}$$

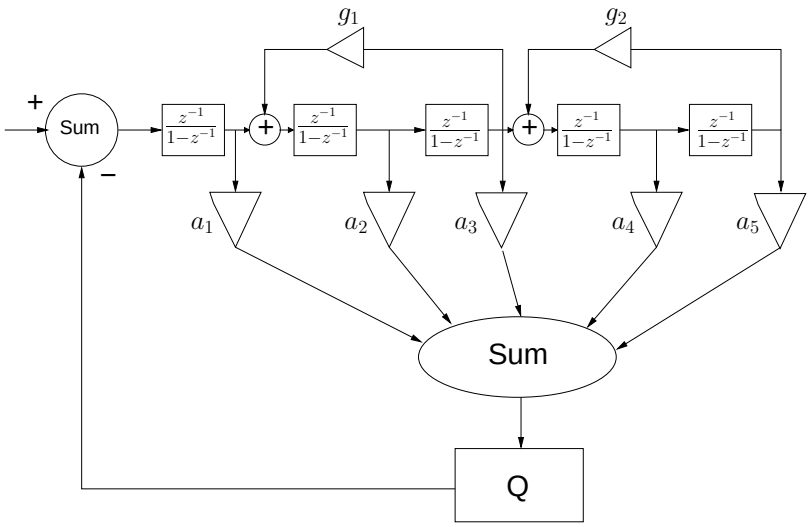

Figure 11. High-order ($N = 5$) SDM: CIFF topology.

The first tap of the impulse response $h^{(N)}(t,\lambda)$ of the warped NTF is

$$h^{(N)}(0,\lambda) = \frac{1}{1+\sum_{k=1}^{N} a_k \Big(\frac{-\lambda}{1+\lambda}\Big)^{p(k)} \prod_{j=1}^{\frac{k-p(k)}{2}} \frac{\lambda^2}{(1+\lambda)^2 - g_j\lambda^2}}. \tag{25}$$

such that the scaled and warped NTF can be written as follows,

$$\tilde{H}^{(N)}(z,\lambda) = \frac{1-\alpha_0}{1+\sum_{k=1}^{N} \alpha_k \Big(\frac{z^{-1}-\lambda}{1-z^{-1}}\Big)^{p(k)} \prod_{j=1}^{\frac{k-p(k)}{2}} \frac{(z^{-1}-\lambda)^2}{(1-z^{-1})^2 - \gamma_j(z^{-1}-\lambda)^2}} \tag{26}$$

with the new feedforward and local resonator feedback coefficients defined by

$$\alpha_k = \frac{a_k}{(1+\lambda)^k}, \qquad k = 1,\ldots,N \tag{27}$$

$$\gamma_j = \frac{g_j}{(1+\lambda)^2}, \qquad j = 1,\ldots,\frac{N-1}{2} \tag{28}$$

and the direct feedforward path coefficient defined as

$$\alpha_0 = -\sum_{k=1}^{N} \alpha_k (-\lambda)^{p(k)} \prod_{j=1}^{\frac{k-p(k)}{2}} \frac{\lambda^2}{1-\gamma_j\lambda^2}. \tag{29}$$

From the scaled and warped NTF in (26), the corresponding L_1 loop filter is calculated using the

leftmost equality in (10), i.e.,

$$\tilde{L}_1^{(N)}(z,\lambda) = \frac{-\alpha_0 - \sum_{k=1}^{N} \alpha_k \Big(\frac{z^{-1}-\lambda}{1-z^{-1}}\Big)^{p(k)} \prod_{j=1}^{\frac{k-p(k)}{2}} \frac{(z^{-1}-\lambda)^2}{(1-z^{-1})^2 - \gamma_j (z^{-1}-\lambda)^2}}{1-\alpha_0}. \tag{30}$$

The next step is to decide in which way the warping should affect the high-order STF, by constraining the L_0 loop filter. A straightforward choice is to put $\tilde{L}_0^{(N)}(z,\lambda) = -\tilde{L}_1^{(N)}(z,\lambda)$, which is similar to the constraint that resulted in the first-order frequency-warped SDM topology I, see (11). In this case, the L_0 loop filter has a transfer function

$$\tilde{L}_{0,\mathrm{I}}^{(N)}(z,\lambda) = \frac{\alpha_0 + \sum_{k=1}^{N} \alpha_k \Big(\frac{z^{-1}-\lambda}{1-z^{-1}}\Big)^{p(k)} \prod_{j=1}^{\frac{k-p(k)}{2}} \frac{(z^{-1}-\lambda)^2}{(1-z^{-1})^2 - \gamma_j (z^{-1}-\lambda)^2}}{1-\alpha_0} \tag{31}$$

hence the corresponding high-order warped STF can be calculated as

$$\tilde{G}_{\mathrm{I}}^{(N)}(z,\lambda) = 1 - \tilde{H}^{(N)}(z,\lambda). \tag{32}$$

The resulting high-order frequency-warped SDM CIFF topology I is shown in Fig. 12. The magnitude response of the NTF and STF is plotted in Figs. 13(a)-(d), for positive and negative values of the warping parameter λ.

It is also possible to derive a different warped high-order topology from (30) which has a scaling factor $1-\lambda$ in the SDM feedback path, similar to the topology II derived in the first-order case (see Section III-A). However, the constraint $\tilde{L}_0(z,\lambda) = L_0(z)$, which was used to derive the first-order topology II, is not very attractive in the high-order case since the loop filters $\tilde{L}_0^{(N)}(z,\lambda)$ and $\tilde{L}_1^{(N)}(z,\lambda)$ would then strongly differ and not share many components. Nevertheless, there is a different way of interpreting the first-order topology II, which does allow for a generalization to the high-order case with preservation of the basic SDM structure (i.e., with $\tilde{L}_0^{(N)}(z,\lambda)$ and $\tilde{L}_1^{(N)}(z,\lambda)$ sharing most of their components). By comparing the first-order loop filter expressions in (10) and (14), the first-order topology II can also be derived by using the constraint

$$\tilde{L}_0(z,\lambda) = -\frac{1}{1-\lambda}\tilde{L}_1(z,\lambda). \tag{33}$$

Before the constraint in (33) can be applied to the high-order SDM design, a factor $(1-\lambda)$ from the warped L_1 loop filter transfer function in (30) has to be extracted. In the Appendix, it is shown that (30) can be rewritten as follows:

$$\tilde{L}_1^{(N)}(z,\lambda) = \Big(\frac{\lambda-1}{1-\alpha_0}\Big)\frac{z^{-1}}{1-z^{-1}}\left\{\alpha_1 + \sum_{l=1}^{\frac{N-1}{2}}\left(\alpha_{2l+1} + \beta_l \frac{1-z^{-1}}{z^{-1}-\lambda} - \lambda\beta_l\Big(\frac{1-z^{-1}}{z^{-1}-\lambda}\Big)^2\right)\prod_{j=1}^{l}\frac{1}{\big(\frac{1-z^{-1}}{z^{-1}-\lambda}\big)^2 - \gamma_j}\right\} \tag{34}$$

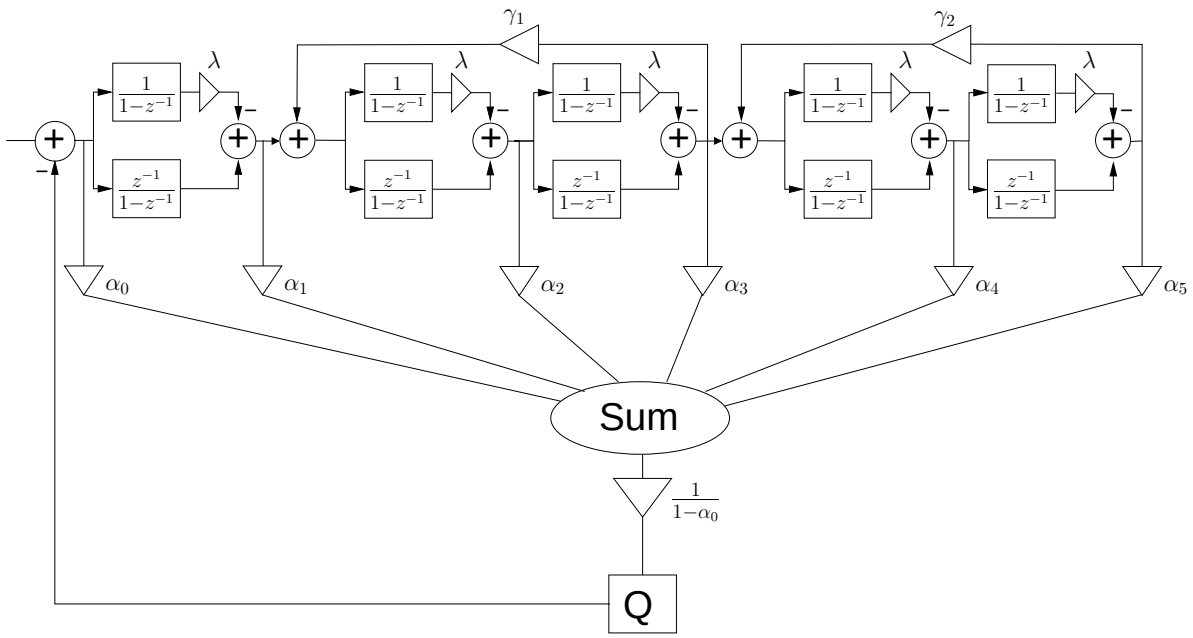

Figure 12. High-order ($N = 5$) frequency-warped SDM: CIFF topology I ($\tilde{L}_0^{(N)}(z,\lambda) = -\tilde{L}_1^{(N)}(z,\lambda)$).

with

$$\beta_l = \sum_{k=2l}^{N} \alpha_k \frac{(-\lambda)^{p(k)}}{\lambda^2} \prod_{j=l}^{\frac{k-p(k)}{2}} \frac{\lambda^2}{1-\gamma_j\lambda^2}. \tag{35}$$

Applying the constraint in (33) to (34) yields the desired topology II expression for the L_0 loop filter,

$$\tilde{L}_{0,\mathrm{II}}^{(N)}(z,\lambda) = \Big(\frac{1}{1-\alpha_0}\Big)\frac{z^{-1}}{1-z^{-1}}\left\{\alpha_1 + \sum_{l=1}^{\frac{N-1}{2}}\left(\alpha_{2l+1} + \beta_l \frac{1-z^{-1}}{z^{-1}-\lambda} - \lambda\beta_l\Big(\frac{1-z^{-1}}{z^{-1}-\lambda}\Big)^2\right)\prod_{j=1}^{l}\frac{1}{\big(\frac{1-z^{-1}}{z^{-1}-\lambda}\big)^2-\gamma_j}\right\} \tag{36}$$

which results in the following STF:

$$\tilde{G}_{\mathrm{II}}^{(N)}(z,\lambda) = \frac{1}{1-\lambda}\big(1-\tilde{H}^{(N)}(z,\lambda)\big). \tag{37}$$

The high-order frequency warped SDM CIFF topology II, as defined by (34) and (36), can be realized as shown in Fig. 14. The following differences with topology I (Fig. 12) can be observed: the first stage of the SDM filter is a traditional integrator instead of a frequency-warped integrator, the odd feedforward coefficients have changed, the feedback path contains a gain factor $1-\lambda$, and finally, $\frac{N-1}{2}$ feedforward branches have been added (which merge with the feedforward branches of the odd stages in case $\gamma_j = 0$). The STF magnitude response is plotted in Figs. 15(a) and 15(b) for positive and negative values of λ, respectively.

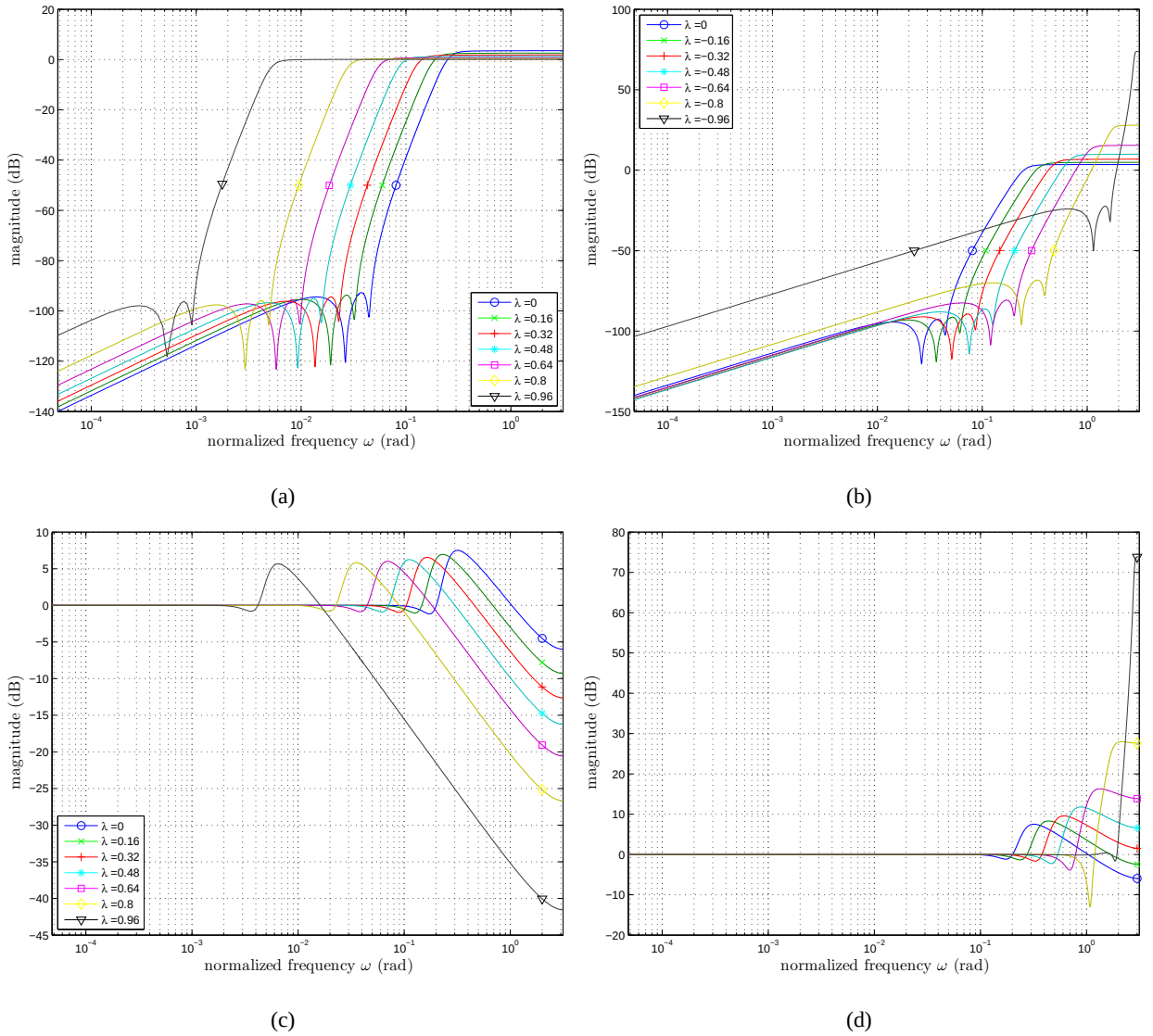

Figure 13. High-order ($N = 5$) frequency-warped SDM CIFF topology I: (a) NTF magnitude response ($\lambda \geq 0$), (b) NTF magnitude response ($\lambda \leq 0$), (c) STF magnitude response ($\lambda \geq 0$), (d) STF magnitude response ($\lambda \leq 0$).

Comparing the NTF frequency responses in Figs. 13(a) and 13(b) with the corresponding responses in the first-order case (Figs. 5(a) and 5(b)), we notice the following. Whereas warping the first-order NTF causes a wideband shift of the SNR curves (towards 0 dB SNR for $\lambda \rightarrow 1$ and towards $-\infty$ for $\lambda \rightarrow -1$), warping the high-order NTF rather results in a noticeable shift of the cut-off frequency (towards dc for $\lambda \rightarrow 1$ and towards the Nyquist frequency for $\lambda \rightarrow -1$). As a consequence, warping the high-order SDM will particularly result in widening ($\lambda > 0$) or narrowing ($\lambda < 0$) the high-frequency band according to which the quantization noise is shaped. Since high-order SDMs are usually applied

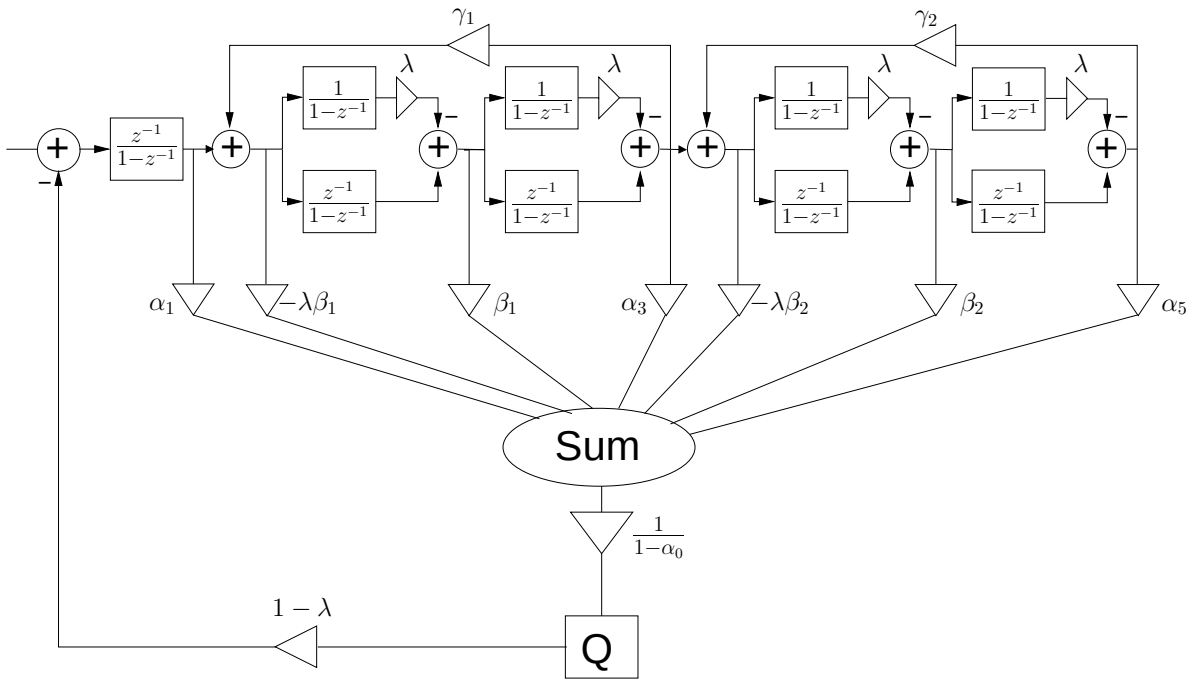

Figure 14. High-order ($N = 5$) frequency-warped SDM: CIFF topology II ($\tilde{L}_0^{(N)}(z,\lambda) = -\frac{1}{1-\lambda}\tilde{L}_1^{(N)}(z,\lambda)$).

to problems featuring a large signal bandwidth [12], e.g. in telecommunications, it is expected to be advantageous to use negative values of the warping parameter. This is confirmed by high-order SDM simulation results presented in Section V-B.

B. Implementation Issues

The high-order frequency-warped SDM CIFF topologies I and II are not realizable in the structure shown in Figs. 12 and 14, respectively, if both $\lambda \neq 0$ and $\gamma_j \neq 0$ for any $j \in \{1, \ldots, (N-1)/2\}$. This is due to the fact that the frequency warping introduces a delay-free path in each stage of the SDM filter, hence when a local feedback with coefficient γ_j is employed, an algebraic loop is created. This is a commonly encountered problem when designing warped IIR (WIIR) filters, and several solutions have been suggested [14]-[16]. The method proposed in [13] may be applied here to transform the non-realizable high-order SDM topologies described above into realizable structures.

The approach is illustrated by considering the j-th section ($j \in \{1, \ldots, (N-1)/2\}$) of the high-order frequency warped SDM CIFF topology II, which is shown in Fig. 16 and consists of an odd and even SDM stage surrounded by a local feedback loop. First of all, this integrator-resonator structure is transformed into a direct-form II WIIR structure, see Fig. 17, which is still non-realizable. In this

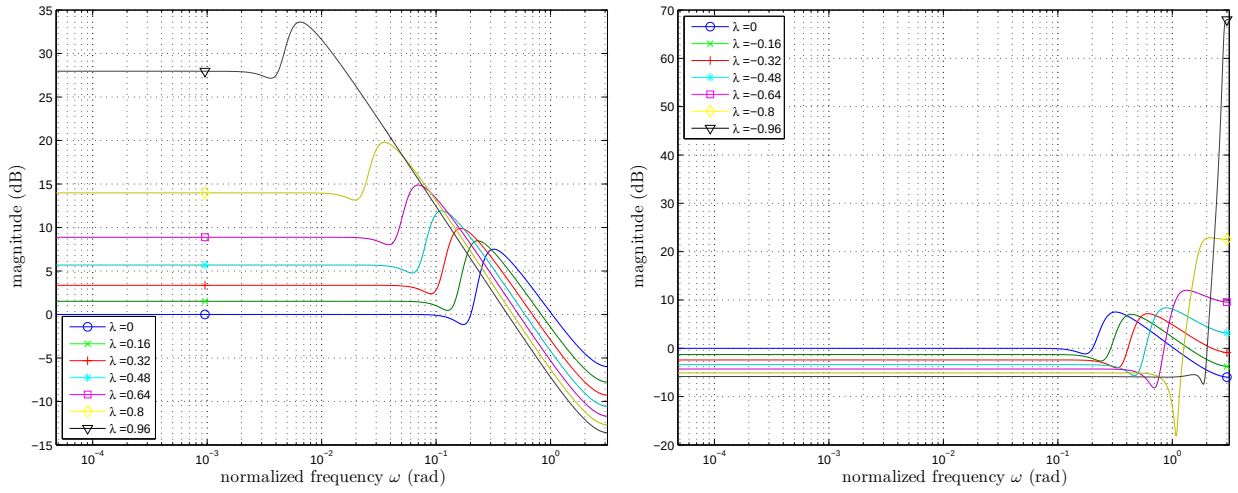

(a) (b)

Figure 15. High-order ($N = 5$) frequency-warped SDM CIFF topology II: (a) STF magnitude response ($\lambda \geq 0$), (b) STF magnitude response ($\lambda \leq 0$).

direct-form structure, the input and output signals of the first, second, and third unit delay element at time t are denoted as $x_0(t)$ and $y_0(t)$, $x_1(t)$ and $y_1(t)$, and $x_2(t)$ and $y_2(t)$, respectively, see Fig. 17. The feedback structure of the non-realizable direct-form II implementation is such that the state variable $x_0(t)$ is a function of the input $x(t)$ and the state variable $x_2(t)$, i.e.,

$$x_0(t) = x(t) + \gamma_j x_2(t). \tag{38}$$

If $x_0(t)$ is instead calculated using the input $x(t)$ and the state variables $y_i(t),\ i = 0, 1, 2$, then a structure without algebraic loops can be obtained. Substituting

$$x_2(t) = y_1(t) + (y_2(t) - \lambda x_1(t)) \tag{39}$$

in (38) and

$$x_1(t) = y_0(t) + (y_1(t) - \lambda x_0(t)) \tag{40}$$

in (39),

$$x_0(t) = \frac{1}{1 - \gamma_j \lambda^2}\big(x(t) - \gamma_j \lambda y_0(t) + \gamma_j(1 - \lambda)y_1(t) + \gamma_j y_2(t)\big) \tag{41}$$

which leads to the realizable structure shown in Fig. 18.

It should be noted that the feedforward branches of the transformed structure in Fig. 18 (with feedforward coefficients $-\lambda\beta_l, \beta_l, \alpha_{2l+1}$) are unchanged as compared to the original structure in Fig. 16. As a consequence, the above approach can equivalently be applied to the high-order frequency warped SDM

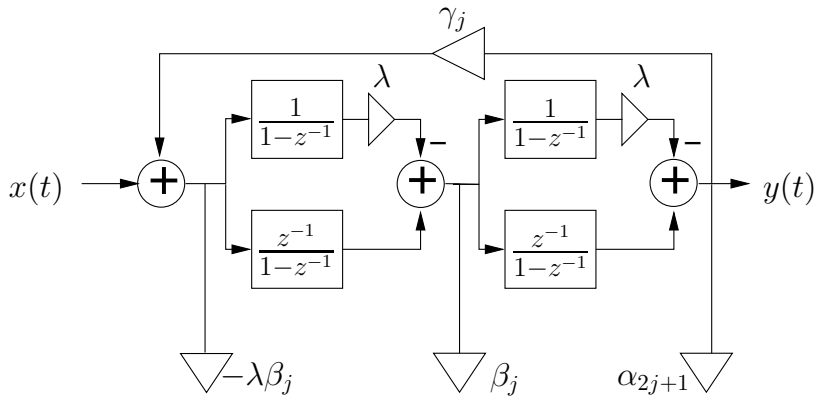

Figure 16. Non-realizable integrator-resonator structure of high-order frequency-warped SDM CIFF topology II section.

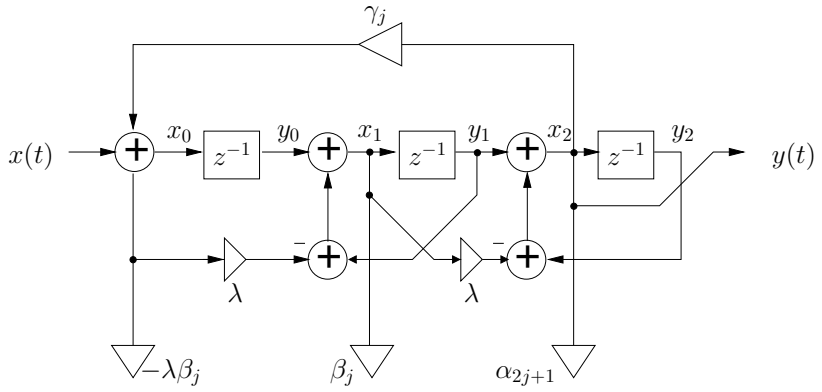

Figure 17. Non-realizable direct-form II WIIR structure of high-order frequency-warped SDM CIFF topology II section.

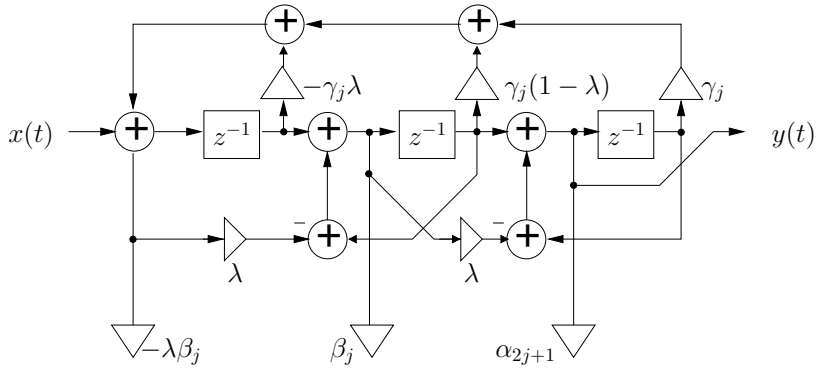

Figure 18. Realizable WIIR structure of high-order frequency-warped SDM CIFF topology II section.

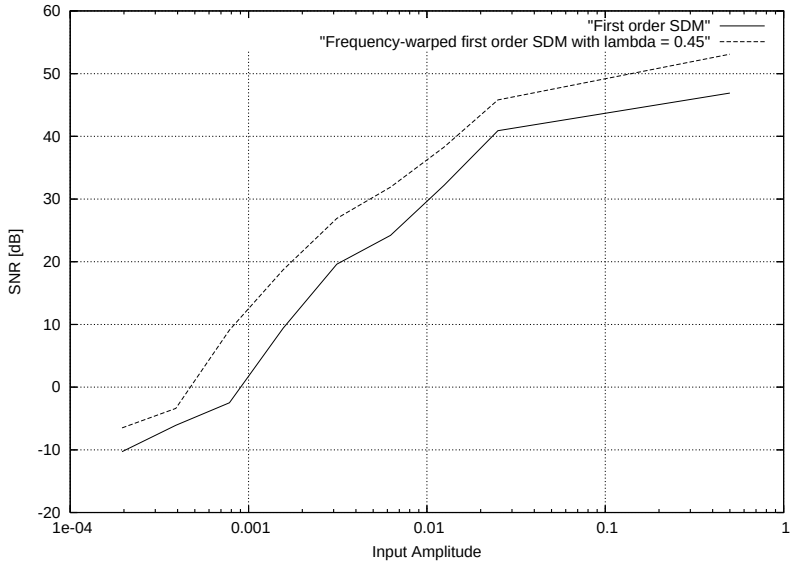

Figure 19. SNR comparison between a first-order traditional SDM and frequency-warped SDM (topology II) for $\lambda = 0.45$.

CIFF topology I, which is made up of similar sections as the one shown in Fig. 16, but with different feedforward branches.

V. Simulation Results

A. First-Order SDM

The positive range $[0, 1)$ of the warping parameter λ is of particular interest for first-order frequency-warped SDMs [10], since it renders the frequency warping perceptually relevant in audio applications [8],[9], and since it yields frequency-warped SDMs of which the NTF frequency response has a smaller out-of-band gain (see Figs. 5(a) and 13(a)), which is beneficial for SDM stability [11]. In Section III-B, it was shown that using the results derived in [10], the SNR is expected to increase for positive λ only when topology II is used.

Extensive simulations of more than $3 \cdot 10^6$ samples were run with sinusoidal input signals of variable amplitude, and with $f_0 = 1$ kHz. The signal bandwidth was $f_B = 24$ kHz and the OSR $= 64$, resulting in a sampling frequency $f_S = 3072$ kHz. The plot representing the SNR for both the traditional SDM and the frequency-warped SDM is shown in Fig. 19. For several positive values of the warping parameter λ we have found an improved SNR performance as compared to the traditional SDM, with an optimum average 6 dB gain for $\lambda = 0.45$.

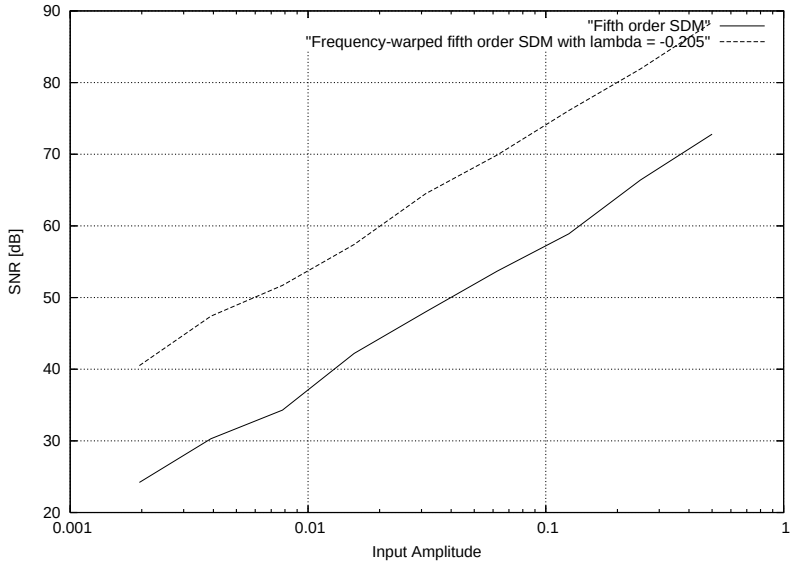

Figure 20. SNR comparison between a fifth-order traditional SDM and frequency-warped SDM (topology II) for $\lambda = -0.205$.

B. High-Order SDM

As for the first-order case, a set of simulations were run for a fifth-order frequency-warped SDM CIFF topology II with sinusoidal input signals of variable amplitude and with $f_0 = 1$ kHz. Again, $f_B = 24$ kHz and OSR $= 64$, such that $f_S = 3072$ kHz. The plot representing the SNR for both the traditional SDM and the frequency-warped SDM is shown in Fig. 20. Also in the case of high-order SDM the simulation results show that frequency-warping leads to an improvement in the SNR performance, in this case for negative values of the warping parameter λ, with an optimum average 14 dB gain for $\lambda = -0.205$.

The SDM filter coefficients used in the simulation are obtained as follows: First, a fifth-order NTF is synthesized by placing all zeros at $z = 1$, using the method in [5, Ch. 8]. This NTF is then converted into a CIFF topology with a unit STF, which yields the feedforward and local resonator feedback coefficients: $a_1 = 0.80901, a_2 = 0.31489, a_3 = 0.072124, a_4 = 0.0096177, a_5 = 0.00051673$ and $g_1 = g_2 = 0$. Finally, the α_k and γ_j coefficients for the frequency-warped SDM CIFF topology I are calculated using (27) and (28),and the β_l coefficients for topology II are obtained using (35).

VI. CONCLUSION

We proposed an SDM design procedure that applies frequency warping to the noise transfer function and to the signal stransfer function independently, allowing to produce several SDM topologies that could be useful in different applications. The simple first-order example is typical of audio applications while

the more complex fifth-order example could be applicable in telecommunication applications to improve the performance of existing systems. In each case we explored both positive and negative values of the warping parameter λ, obtaining in both cases a better SNR performance. Extensive simulations were run to validate the proposed models and their results are worth noticing: In the first-order case an optimum 6 dB gain was obtained for a positive value of $\lambda = 0.45$ and for the fifth-order case an optimum 14 dB gain was obtained for a negative value of $\lambda = -0.205$.

ACKNOWLEDGEMENTS

This research work was carried out at the ESAT laboratory of the Katholieke Universiteit Leuven, in the frame of the Edith Program, the K.U.Leuven Research Council: CoE EF/05/006 Optimization in Engineering (OPTEC), and the Belgian Programme on Interuniversity Attraction Poles, initiated by the Belgian Federal Science Policy Office IUAP P6/04 (DYSCO, "Dynamical systems, control and optimization", 2007-2011) and was supported by the Marie Curie Early Stage Training No. 504125 and the Institute for the Promotion of Innovation through Science and Technology in Flanders (IWT-Vlaanderen). The scientific responsibility is assumed by its authors.

APPENDIX

CALCULUS FOR HIGH-ORDER FREQUENCY-WARPED SDM CIFF TOPOLOGY II

The aim is to extract a factor $(1-\lambda)$ from the high-order warped L_1 loop filter transfer function given in (30). By substituting (29) in (30),

$$\tilde{L}_1^{(N)}(z,\lambda) = \frac{\displaystyle\sum_{k=1}^{N} \alpha_k (-\lambda)^{p(k)} \prod_{j=1}^{\frac{k-p(k)}{2}} \frac{\lambda^2}{1-\gamma_j\lambda^2} - \sum_{k=1}^{N} \alpha_k \Big(\frac{z^{-1}-\lambda}{1-z^{-1}}\Big)^{p(k)} \prod_{j=1}^{\frac{k-p(k)}{2}} \frac{(z^{-1}-\lambda)^2}{(1-z^{-1})^2-\gamma_j(z^{-1}-\lambda)^2}}{1-\alpha_0}$$

$$= \frac{1}{1-\alpha_0} \sum_{k=1}^{N} \alpha_k \left[(-\lambda)^{p(k)} \prod_{j=1}^{\frac{k-p(k)}{2}} \frac{\lambda^2}{1-\gamma_j\lambda^2} - \frac{1}{\big(\frac{1-z^{-1}}{z^{-1}-\lambda}\big)^{p(k)}} \prod_{j=1}^{\frac{k-p(k)}{2}} \frac{1}{\big(\frac{1-z^{-1}}{z^{-1}-\lambda}\big)^2-\gamma_j} \right]. \tag{42}$$

The two terms between square brackets in (42) can be rewritten with a common denominator as follows:

$$\tilde{L}_1^{(N)}(z,\lambda) = \frac{1}{1-\alpha_0} \sum_{k=1}^{N} \alpha_k \frac{\Big(-\lambda\frac{1-z^{-1}}{z^{-1}-\lambda}\Big)^{p(k)} \prod_{j=1}^{\frac{k-p(k)}{2}} \lambda^2 \Big(\big(\frac{1-z^{-1}}{z^{-1}-\lambda}\big)^2-\gamma_j\Big) - \prod_{j=1}^{\frac{k-p(k)}{2}} (1-\gamma_j\lambda^2)}{\Big(\frac{1-z^{-1}}{z^{-1}-\lambda}\Big)^{p(k)} \prod_{j=1}^{\frac{k-p(k)}{2}} (1-\gamma_j\lambda^2)\Big(\big(\frac{1-z^{-1}}{z^{-1}-\lambda}\big)^2-\gamma_j\Big)}. \tag{43}$$

The leftmost product term in the numerator can be expanded as follows:

$$\prod_{j=1}^{\frac{k-p(k)}{2}} \lambda^2\Big(\Big(\frac{1-z^{-1}}{z^{-1}-\lambda}\Big)^2-\gamma_j\Big) = \prod_{j=1}^{\frac{k-p(k)}{2}} \Big(\Big(-\lambda\frac{1-z^{-1}}{z^{-1}-\lambda}\Big)^2-1+1-\gamma_j\lambda^2\Big) \tag{44}$$

$$= \Big(\Big(-\lambda\frac{1-z^{-1}}{z^{-1}-\lambda}\Big)^2-1\Big)\prod_{j=2}^{\frac{k-p(k)}{2}} \lambda^2\Big(\Big(\frac{1-z^{-1}}{z^{-1}-\lambda}\Big)^2-\gamma_j\Big) + (1-\gamma_1\lambda^2)\prod_{j=2}^{\frac{k-p(k)}{2}} \Big(\Big(-\lambda\frac{1-z^{-1}}{z^{-1}-\lambda}\Big)^2-\gamma_j\lambda^2\Big).$$

The rightmost product term in the latter equation can be expanded in a similar way, and this process can be repeated to obtain

$$\prod_{j=1}^{\frac{k-p(k)}{2}} \lambda^2\Big(\Big(\frac{1-z^{-1}}{z^{-1}-\lambda}\Big)^2-\gamma_j\Big) \tag{45}$$

$$= \Big(\Big(-\lambda\frac{1-z^{-1}}{z^{-1}-\lambda}\Big)^2-1\Big)\sum_{l=1}^{\frac{k-p(k)}{2}}\Big(\prod_{j=1}^{l-1}(1-\gamma_j\lambda^2)\prod_{j=l+1}^{\frac{k-p(k)}{2}}\lambda^2\Big(\Big(\frac{1-z^{-1}}{z^{-1}-\lambda}\Big)^2-\gamma_j\Big)\Big) + \prod_{j=1}^{\frac{k-p(k)}{2}}(1-\gamma_j\lambda^2).$$

which after substitution in (43) leads to

$$\tilde{L}_1^{(N)}(z,\lambda) = \frac{1}{1-\alpha_0}\sum_{k=1}^{N}\alpha_k\Bigg\{\frac{\Big(\Big(-\lambda\frac{1-z^{-1}}{z^{-1}-\lambda}\Big)^{p(k)}-1\Big)\prod_{j=1}^{\frac{k-p(k)}{2}}(1-\gamma_j\lambda^2)}{\Big(\frac{1-z^{-1}}{z^{-1}-\lambda}\Big)^{p(k)}\prod_{j=1}^{\frac{k-p(k)}{2}}(1-\gamma_j\lambda^2)\Big(\Big(\frac{1-z^{-1}}{z^{-1}-\lambda}\Big)^2-\gamma_j\Big)} \tag{46}$$

$$+\frac{\Big(-\lambda\frac{1-z^{-1}}{z^{-1}-\lambda}\Big)^{p(k)}\Big(\Big(-\lambda\frac{1-z^{-1}}{z^{-1}-\lambda}\Big)^2-1\Big)\sum_{l=1}^{\frac{k-p(k)}{2}}\Big(\prod_{j=1}^{l-1}(1-\gamma_j\lambda^2)\prod_{j=l+1}^{\frac{k-p(k)}{2}}\lambda^2\Big(\Big(\frac{1-z^{-1}}{z^{-1}-\lambda}\Big)^2-\gamma_j\Big)\Big)}{\Big(\frac{1-z^{-1}}{z^{-1}-\lambda}\Big)^{p(k)}\prod_{j=1}^{\frac{k-p(k)}{2}}(1-\gamma_j\lambda^2)\Big(\Big(\frac{1-z^{-1}}{z^{-1}-\lambda}\Big)^2-\gamma_j\Big)}\Bigg\}.$$

Recognizing that

$$\Big(-\lambda\frac{1-z^{-1}}{z^{-1}-\lambda}\Big)^2-1 = \Big(-\lambda\frac{1-z^{-1}}{z^{-1}-\lambda}-1\Big)\Big(-\lambda\frac{1-z^{-1}}{z^{-1}-\lambda}+1\Big), \tag{47}$$

$$\Big(-\lambda\frac{1-z^{-1}}{z^{-1}-\lambda}\Big)^{p(k)}-1 = p(k)\Big(-\lambda\frac{1-z^{-1}}{z^{-1}-\lambda}-1\Big) \tag{48}$$

and

$$-\lambda\frac{1-z^{-1}}{z^{-1}-\lambda}-1 = (\lambda-1)\frac{z^{-1}}{z^{-1}-\lambda} \tag{49}$$

(46) can be rewritten as follows:

$$\tilde{L}_1^{(N)}(z,\lambda) = \Big(\frac{\lambda-1}{1-\alpha_0}\Big)\frac{z^{-1}}{z^{-1}-\lambda}\sum_{k=1}^{N}\alpha_k\left\{\frac{p(k)}{\big(\frac{1-z^{-1}}{z^{-1}-\lambda}\big)^{p(k)}}\prod_{j=1}^{\frac{k-p(k)}{2}}\frac{1}{\big(\frac{1-z^{-1}}{z^{-1}-\lambda}\big)^2-\gamma_j}\right. \tag{50}$$

$$\left.+(-\lambda)^{p(k)}\Big(-\lambda\frac{1-z^{-1}}{z^{-1}-\lambda}+1\Big)\sum_{l=1}^{\frac{k-p(k)}{2}}\prod_{j=l}^{\frac{k-p(k)}{2}}\frac{1}{1-\gamma_j\lambda^2}\prod_{j=1}^{l}\frac{\lambda^{2(\frac{k-p(k)}{2}-l)}}{\big(\frac{1-z^{-1}}{z^{-1}-\lambda}\big)^2-\gamma_j}\right\}.$$

The expression in (50) can be organized in a different way by changing the order of the summations and by grouping the product terms involving $\big(\big(\frac{1-z^{-1}}{z^{-1}-\lambda}\big)^2-\gamma_j\big)^{-1}$ that have equal upper limits, i.e.,

$$\tilde{L}_1^{(N)}(z,\lambda) = \Big(\frac{\lambda-1}{1-\alpha_0}\Big)\frac{z^{-1}}{z^{-1}-\lambda}\left\{\alpha_1\frac{z^{-1}-\lambda}{1-z^{-1}}\right. \tag{51}$$

$$\left.+\sum_{l=1}^{\frac{N-1}{2}}\left(\alpha_{2l+1}\frac{z^{-1}-\lambda}{1-z^{-1}}+\sum_{k=2l}^{N}\alpha_k\Big(-\lambda\frac{1-z^{-1}}{z^{-1}-\lambda}+1\Big)\frac{(-\lambda)^{p(k)}}{\lambda^2}\prod_{j=l}^{\frac{k-p(k)}{2}}\frac{\lambda^2}{1-\gamma_j\lambda^2}\right)\prod_{j=1}^{l}\frac{1}{\big(\frac{1-z^{-1}}{z^{-1}-\lambda}\big)^2-\gamma_j}\right\}.$$

Finally, a factor $\frac{z^{-1}-\lambda}{1-z^{-1}}$ can be extracted from the braces in (51) to obtain

$$\tilde{L}_1^{(N)}(z,\lambda) = \Big(\frac{\lambda-1}{1-\alpha_0}\Big)\frac{z^{-1}}{1-z^{-1}}\left\{\alpha_1+\sum_{l=1}^{\frac{N-1}{2}}\left(\alpha_{2l+1}+\beta_l\frac{1-z^{-1}}{z^{-1}-\lambda}-\lambda\beta_l\Big(\frac{1-z^{-1}}{z^{-1}-\lambda}\Big)^2\right)\prod_{j=1}^{l}\frac{1}{\big(\frac{1-z^{-1}}{z^{-1}-\lambda}\big)^2-\gamma_j}\right\} \tag{52}$$

with

$$\beta_l = \sum_{k=2l}^{N}\alpha_k\frac{(-\lambda)^{p(k)}}{\lambda^2}\prod_{j=l}^{\frac{k-p(k)}{2}}\frac{\lambda^2}{1-\gamma_j\lambda^2}. \tag{53}$$

REFERENCES

[1] J. Candy and G. Temes, Eds., *Oversampling Delta-Sigma Data Converters: Theory, Design, and Simulation*. Piscataway, NJ: IEEE Press, 1992.

[2] R. Schreier, "An empirical study of high-order single-bit delta-sigma modulators," *IEEE Trans. Circuits Syst. II, Analog Digit. Signal Process.*, vol. 40, no. 8, pp. 461–466, Aug. 1993.

[3] P. M. Aziz, H. V. Sorensen, and J. van der Spiegel, "An overview of sigma-delta converters," *IEEE Signal Process. Mag.*, vol. 13, no. 1, pp. 61–84, Jan. 1996.

[4] R. W. Adams, "The design of high-order single-bit $\Delta\Sigma$ ADCs," in *Delta-Sigma Data Converters: Theory, Design, and Simulation*, S. R. Norsworthy, R. Schreier, and G. C. Temes, Eds. Piscataway, NJ: IEEE Press, 1997, ch. 5.

[5] R. Schreier and G. C. Temes, *Understanding Delta-Sigma Data Converters*. New York: Wiley-IEEE Press, 2005.

[6] A. V. Oppenheim, D. H. Johnson, and K. Steiglitz, "Computation of spectra with unequal resolution using the fast Fourier transform," *Proc. IEEE*, vol. 59, no. 2, pp. 299–301, Feb. 1971.

[7] A. Härmä, M. Karjalainen, L. Savioja, V. Välimäki, U. K. Laine, and J. Huopaniemi, "Frequency-warped signal processing for audio applications," *J. Audio Eng. Soc.*, vol. 48, no. 11, pp. 1011–1031, Nov. 2000.

[8] A. Härmä and U. K. Laine, "A comparison of warped and conventional linear predictive coding," *IEEE Trans. Speech Audio Process.*, vol. 9, no. 5, pp. 579–588, July 2001.

[9] J. O. Smith and J. S. Abel, “Bark and ERB bilinear transforms,” *IEEE Trans. Speech Audio Process.*, vol. 7, no. 6, pp. 697–708, Nov. 1999.

[10] L. Ausiello, T. van Waterschoot, and M. Moonen, “A first-order frequency-warped sigma delta modulator with improved signal-to-noise ratio,” submitted for publication in *Proc. 16th European Signal Process. Conf. (EUSIPCO ’08)*, Lausanne, Switzerland. ESAT-SISTA Technical Report TR 08-10, Katholieke Universiteit Leuven, Belgium, Feb. 2008. [Online]. Available: ftp://ftp.esat.kuleuven.be/pub/sista/vanwaterschoot/abstracts/08-10.html

[11] R. W. Adams and R. Schreier, “Stability theory for $\Delta\Sigma$ modulators,” in *Delta-Sigma Data Converters: Theory, Design, and Simulation*, S. R. Norsworthy, R. Schreier, and G. C. Temes, Eds. Piscataway, NJ: IEEE Press, 1997, ch. 4.

[12] M. A. Al-Alaoui and R. Ferzli, “An enhanced first-order sigma-delta modulator with a controllable signal-to-noise ratio,” *IEEE Trans. Circuits Syst.*, vol. 53, no. 3, pp. 634–643, Mar. 2006.

[13] M. Karjalainen, A. Härmä, and U. K. Laine, “Realizable warped IIR filters and their properties,” in *Proc. 1997 IEEE Int. Conf. Acoust., Speech, Signal Process. (ICASSP ’97)*, vol. 3, Munich, Germany, Apr. 1997, pp. 2205–2208.

[14] H. W. Strube, “Linear prediction on a warped frequency scale,” *J. Acoust. Soc. Amer.*, vol. 68, no. 4, pp. 1071–1076, Oct. 1980.

[15] K. Steiglitz, “A note on variable recursive digital filters,” *IEEE Trans. Acoust., Speech, Signal Process.*, vol. ASSP-28, no. 1, pp. 111–112, Feb. 1980.

[16] A. Härmä, “Implementation of frequency-warped recursive filters,” *Signal Processing*, vol. 80, no. 3, pp. 543–548, Mar. 2000.